



From critical behavior to catastrophic runaways: comparing sheared granular materials with bulk metallic glasses

Alan A. Long¹ · Dmitry V. Denisov² · Peter Schall² · Todd C. Hufnagel³ · Xiaojun Gu⁴ · Wendelin J. Wright^{4,5} · Karin A. Dahmen¹

Received: 13 May 2019 / Published online: 20 September 2019
© The Author(s) 2019

Abstract

The flow of granular materials and metallic glasses is governed by strongly correlated, avalanche-like deformation. Recent comparisons focused on the scaling regimes of the small avalanches, where strong similarities were found in the two systems. Here, we investigate the regime of large avalanches by computing the temporal profile or “shape” of each one, i.e., the time derivative of the stress-time series during each avalanche. We then compare the experimental statistics and dynamics of these shapes in granular media and bulk metallic glasses. We complement the experiments with a mean-field model that predicts a critical size beyond which avalanches turn into large runaway events. We find that this transition is reflected in a characteristic change of the peak width of the avalanche profile from broad to narrow, and we introduce a new metric for characterizing this dynamic change. The comparison of the two systems points to the same deformation mechanism in both metallic glasses and granular materials.

Keywords Granular materials · Bulk metallic glasses · Avalanches · Critical behavior · Scaling behavior

1 Introduction

Many diverse materials systems show intermittent plasticity. Bulk metallic glasses (BMGs) [1–3], granular materials [3–6], high entropy alloys [7], and nanocrystals [3, 8, 9] all show characteristics of discrete flow. Numerous groups have undertaken modeling, simulations, and experimental studies

to determine whether these discrete plastic events show the same statistics and dynamics, irrespective of the microscopic details [1–24]. Understanding the details of the mechanisms for these behaviors is critical to safely using these materials in applications and developing microstructural design principles to tailor mechanical properties. Proper measurement of avalanche behavior requires exceptionally low noise and high temporal resolution data, which can be laborious to obtain. Nanocrystals require time consuming and costly specimen preparation to produce micro- or nanopillars for compression testing and often suffer from significant stress concentrations where the pillars contact the loading surface. High entropy alloys rarely show measurable avalanche behavior at room temperature. Recently the requisite experimental techniques to study these discrete events often called “avalanches” have been applied to BMGs and granular materials, and these systems are the focus of the present work.

Both metallic glasses and granular materials show two types of avalanches that have been previously classified as “small” and “large.” Small avalanches slip progressively in small increments and cluster together in time. They are microscopic and power-law distributed in size and other metrics. In contrast, large avalanches recur quasi-periodically and span the entire system in the form of shear bands

This article is part of the Topical Collection: In Memoriam of Robert P. Behringer.

✉ Karin A. Dahmen
dahmen@illinois.edu

¹ Department of Physics and Institute of Condensed Matter Theory, University of Illinois at Urbana Champaign, 1110 West Green Street, Urbana, IL 61801, USA

² Van der Waals-Zeeman Institute, University of Amsterdam, Science Park 904, 1098 XH Amsterdam, The Netherlands

³ Department of Materials Science and Engineering, Johns Hopkins University, 3400 North Charles Street, Baltimore, MD 21218-2608, USA

⁴ Department of Mechanical Engineering, One Dent Drive, Bucknell University, Lewisburg, PA 17837, USA

⁵ Department of Chemical Engineering, One Dent Drive, Bucknell University, Lewisburg, PA 17837, USA

[1, 10]. The small and large avalanches are interspersed in time throughout plastic deformation (see [25] for simulations from Cao et al. to aid visualization).

In a number of studies on both BMGs and granular materials, the avalanche statistics are consistent with the predictions of the same mean-field model [1–8, 10, 14, 15, 18, 25–28]. The power-law scaling behavior for the small avalanches agrees with the mean-field predictions in both systems (within statistical error bars). Mean-field behavior as described here is expected when there is shear localization [10, 15] as is the case in many of the cited experiments. A number of simulations in the absence of shear bands give other scaling behaviors [29]. Here we focus especially on the large avalanches that span the entire system. These avalanches manifest as macroscopic slips of shear bands in metallic glasses and granular materials, similar to catastrophic earthquakes or landslides on a larger scale. These large avalanches make deformation difficult to control and limit the usefulness of these materials. In this work, we examine the temporal profile or “shape” of the large avalanches, i.e., the time derivative of the stress-time series during each avalanche. The objective is to compare the statistics of large avalanches in granular media and BMGs with model predictions. The results show good agreement between the behavior of BMGs, granular materials, and the predictions of the mean-field model.

1.1 Mean-field model

We model slip avalanches in BMGs and granular materials using a mean-field approach, in which the deforming material is divided into N cells [6, 15]. Each cell has its own failure threshold. As the system is deformed, the local shear stresses increase until they reach the local failure stress. At the failure stress, the failed cell slips forward by a discrete amount (the amount for each cell is random). Consequently, the released stress is distributed to the other cells and the spring that externally loads the system. This released stress can cause some of the other cells to fail. Each slip thus can, in turn, lead to further failures, resulting in a cascade or avalanche of failures. Such a slip avalanche is observed as a stress drop under displacement control or a strain jump under load control. For both BMGs and granular materials, it is important to include threshold weakening in the model, i.e., a threshold can be lowered, by a local slip due to the local dilation it causes [6, 15]. The mean-field model provides analytic predictions for the avalanche statistics, including the distribution of avalanche sizes and durations, their temporal profiles, and spatio-temporal correlations. In the following, we compare some of the model predictions to experiments in granular materials and in BMGs.

1.2 BMG experiment and methodology

$\text{Zr}_{45}\text{Hf}_{12}\text{Nb}_5\text{Cu}_{15.4}\text{Ni}_{12.6}\text{Al}_{10}$ BMG was cut into rectangular specimens with dimensions of 6 mm along the loading axis and a cross-sectional area of 1.5 mm \times 2 mm. An Instron 5584 mechanical test system was used to quasi-statically compress the specimen at a constant displacement rate with a nominal strain rate of 10^{-4} s^{-1} . A 60-kN Kistler piezoelectric load cell recorded the applied force at a data acquisition rate of 100 kHz. See [5] for a schematic diagram and [1] for other details. The avalanches in the specimen were identified, characterized, and measured using previously established methods [1, 26]. Of particular interest are the total stress drop S during an event (which is its “size”), the total duration t of the event (the “duration”), and the maximum magnitude M of the time derivative of the stress-time trace during the avalanche (the “maximum stress drop rate”). Additionally, we calculated the time derivative (i.e., the “temporal profile” or “shape”) of the stress-time series at all times during each avalanche.

1.3 Granular experiment and methodology

For the granular system, we used $\sim 3 \times 10^5$ polymethyl methacrylate spheres with a diameter of 1.5 mm and polydispersity of $\sim 5\%$, placed in a shear cell with tilting side walls and confining top plate (again see [5] for a schematic diagram). The weight of the top plate exerted a confining normal pressure of 9.6 kPa on the granular material, causing it to adopt a volume fraction of $\sim 60\%$ under the applied slow shear, as determined by direct particle counting. We sheared the material at a constant shear rate of $\sim 9.1 \times 10^{-4} \text{ s}^{-1}$ to a total strain of $\gamma = 20\%$. Built-in pressure sensors in the tilting walls of the shear cell recorded the force fluctuations at a temporal resolution of 2 ms [4]. We measured the force drops to resolve the dynamics of the slip events and identify their size and duration. The temporal resolution is sufficient to reconstruct the entire temporal profile of granular avalanches in the same way as in the BMG experiments [5].

2 Results and discussion

Previous studies [1–5] indicate that both BMGs and granular materials show avalanche statistics that are consistent with the predictions of the mean-field model with threshold weakening; we also see both similar statistics and similar dynamics for large and small avalanches in BMGs and granular materials [5]. This is shown by plotting the duration T of each avalanche versus avalanche size S in Fig. 1a for BMGs and Fig. 1c for granular media. The mean-field prediction,

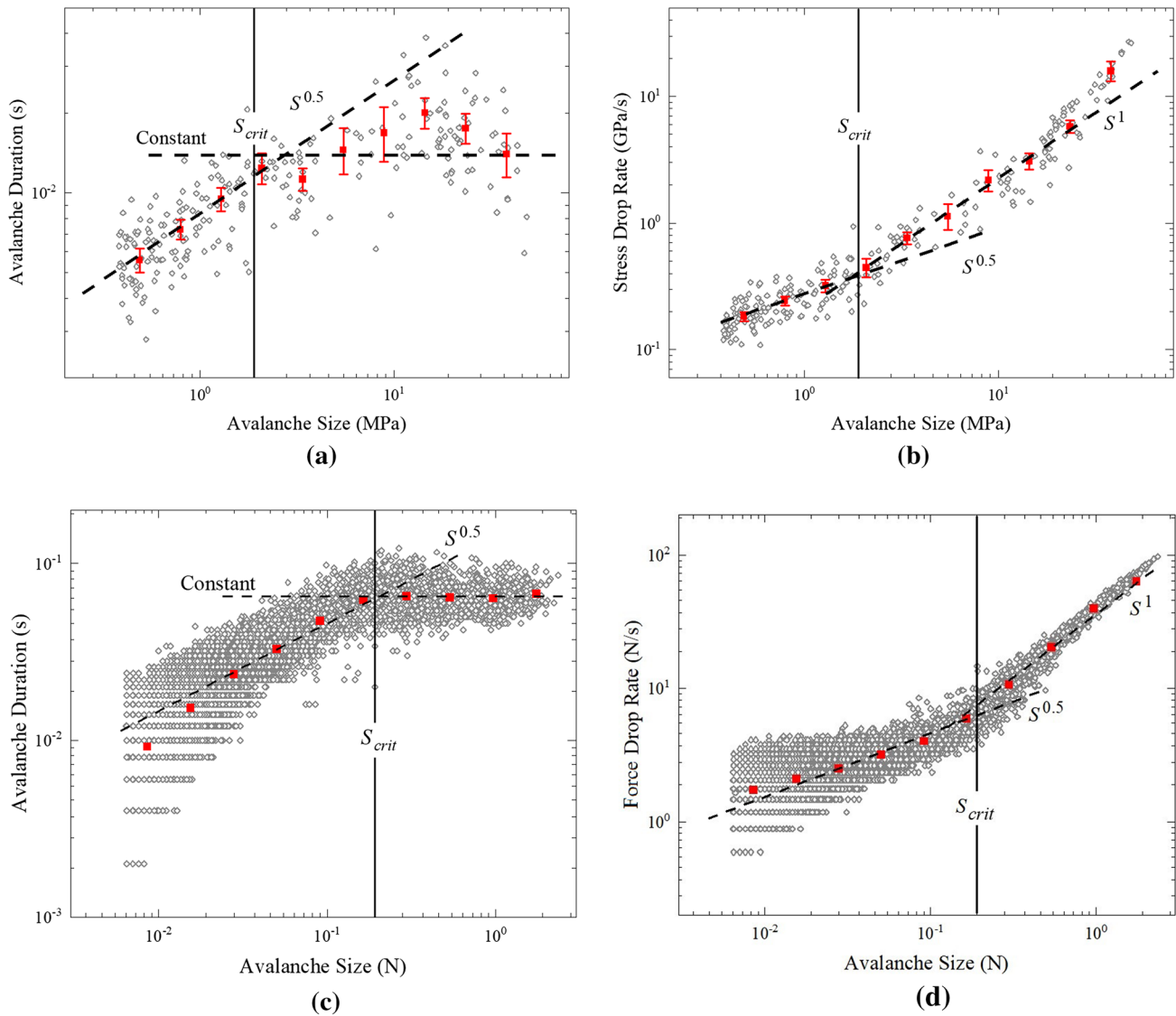


Fig. 1 Avalanche duration and maximum drop rate plotted against size for bulk metallic glasses, **a** and **b** respectively, and for granular media, **c** and **d**, respectively. The 1/2 power laws are the mean-field predictions for the small avalanches in all graphs. S_{crit} is the end of the scaling regime for the size distribution and represents the critical size that separates the small and large events. $S_{crit}=2$ MPa for BMGs and $S_{crit}=0.2$ N for granular materials. The large events have different

dynamics than the avalanches in the scaling regime as predicted by the mean-field model [6, 15]. These large events have similar power-law exponents of 1 in both systems. The squares indicate average duration (**a, c**) or average maximum drop rate (**b, d**) in one of 10 size bins. Error bars indicate 95% confidence intervals. The error bars are on the order of the marker size in **c** and **d**

a power-law relation $T \sim S^{\sigma \nu z}$ with exponent $\sigma \nu z = 1/2$ for the small avalanches in the power-law scaling regime, is indicated by a dashed line. Indeed, both systems follow this scaling for avalanche sizes smaller than a critical size, which is about 2 MPa for BMGs and 0.2 N for the granular system, but for stress drops or force drops larger than these critical sizes, they do not. We denote the critical size as approximate; the model predicts [15] there is a (first-order) transition from small to large avalanches that is spread over a finite range of avalanche sizes due to the disorder in the samples. We specify fixed values here that are consistent with all of

the figures in this paper for which some transitions appear sharper than others (e.g., compare Fig. 1a, c and also b, d).

The model predicts that above the critical size, the dynamics change, causing avalanches to turn into runaway events that span the entire system. In the large-avalanche regime, the durations decrease with avalanche size (BMGs), or they are roughly independent of size (granular system). We address this difference in forthcoming work. The model predicts that the critical size depends on how much the system weakens during a slip. In the model we assume that the thresholds to slipping are lowered relative to their initial

value by an amount proportional to the weakening parameter ϵ . The model further assumes that the thresholds reheel during the time between avalanches to their initial strengths. The model predicts that avalanches that are larger than a critical size $S_{crit} \sim 1/\epsilon^2$ become large “runaway” events that extend across the entire specimen as fully developed shear bands. The weakening dependence $S_{crit} \sim 1/\epsilon^2$ implies that as the weakening ϵ becomes larger, the critical size S_{crit} becomes smaller [15]. Brittle materials have greater weakening than ductile materials.

The maximum stress (or load) drop rate during an avalanche shows similar trends. For the small avalanches, i.e., those in the power-law scaling regime of the avalanche size distribution, the maximum stress drop rate $(-d\sigma/dt)_{max} \sim S^{1/2}$, as predicted by mean-field theory. In contrast, above the critical size, experiments indicate that the maximum stress or force drop rate grows more quickly with avalanche size as shown in Fig. 1b for BMGs, and in Fig. 1d for granular materials. The precise dependence of $(-d\sigma/dt)_{max}$ on S and other statistical properties of the large avalanches should depend on the boundary conditions because the large avalanches span the entire specimen. The boundary conditions are different for the two systems considered here: open boundaries at the specimen sides for BMGs, as opposed to constraints for the granular medium through the box that contains it, which can lead to slight deviations between the large avalanche statistics for both systems.

The observations described above suggest that the dynamics of the small and large avalanches in granular materials and BMGs are related and that the mechanism that determines the critical size separating small from large avalanches is likely similar in both systems. To further understand these behaviors, we look at the propagation dynamics. The mean-field model predicts that the small avalanches in the power-law scaling regime of the avalanche size distribution have self-similar average avalanche profiles. Specifically, the temporal avalanche profiles, averaged over avalanches of the same size, scale as

$$\langle -d\sigma/dt|S \rangle (t) \sim \sqrt{S} G(t/\sqrt{S}) \tag{1}$$

where $G(x)$ is a scaling function [15]. The notation $\langle -d\sigma/dt|S \rangle (t)$ represents the average stress drop rate for avalanches of size S as a function of time t . This prediction has previously been verified experimentally in [1] for BMGs and in granular materials in 3 dimensions [4, 5] and 2 dimensions [27]. If we rescale $G(x)$ such that its maximum value is 1 (which is possible because scaling functions are defined only up to a system dependent pre-factor), then we can rewrite Eq. (1) as

$$\langle -d\sigma/dt|S \rangle (t) \sim M G(t/\sqrt{S}) \tag{2}$$

where $M = \langle (-d\sigma/dt)|S \rangle_{max}$ is the average maximum stress drop rate for avalanches of size S . For small avalanches in

the power-law scaling regime of the avalanche size distribution, Eqs. (1) and (2) together lead to the relation $M \sim \sqrt{S}$. We define the shape index

$$\alpha = \sqrt{S}/M = \sqrt{S}/\langle -d\sigma/dt|S \rangle_{max} \tag{3}$$

to more easily distinguish small from large avalanches. For the small avalanches, this quantity is a constant. For the large system-spanning avalanches, Eq. (1) no longer applies. In this case, mean-field theory predicts that $\alpha \sim 1/\sqrt{S}$ since $M \sim S$ for the large avalanches. To summarize,

$$\alpha \sim \begin{cases} \text{constant}, & S < S_{crit} \\ 1/\sqrt{S}, & S > S_{crit} \end{cases} \tag{4}$$

with a transition region around S_{crit}

We plot α as a function of avalanche size in Figs. 2 and 3. The large avalanches in both BMGs (Fig. 2) and the granular system (Fig. 3) show good agreement with the prediction of Eq. (4), indicating similar dynamics. BMGs have a constant shape index for the small avalanches as predicted. Similarly, for the granular material, α is nearly constant for the small avalanches. The scatter and minor drift of the shape index from the constant value in the small avalanche regime is most likely caused by the discrete durations of the small avalanches very close to the experimental detection threshold. The faster than $1/\sqrt{S}$ decay of the shape index for the very largest BMG avalanches is likely due to greater accumulated weakening for these avalanches shortly before the sample fails.

Changes in the size index correspond to changes in the propagation dynamics. This can be seen experimentally in

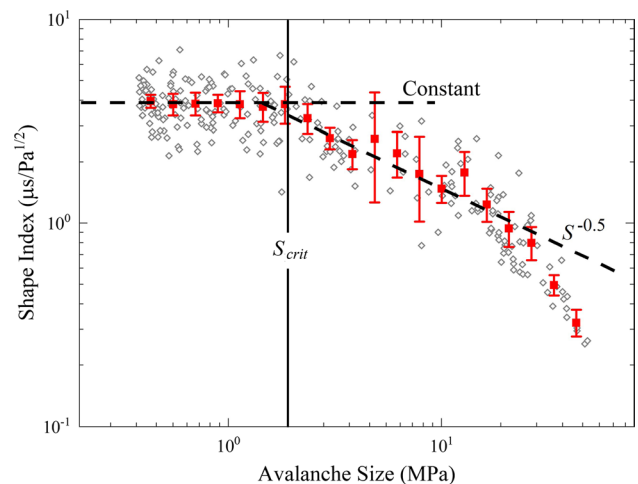


Fig. 2 Shape index α for bulk metallic glasses. The shape index characterizes the propagation dynamics. It is constant for the small avalanches. Above the critical size ($S > 2$ MPa), we see an approximate $-1/2$ power-law dependence. The squares indicate the average shape index in one of 20 size bins. Error bars indicate 95% confidence intervals

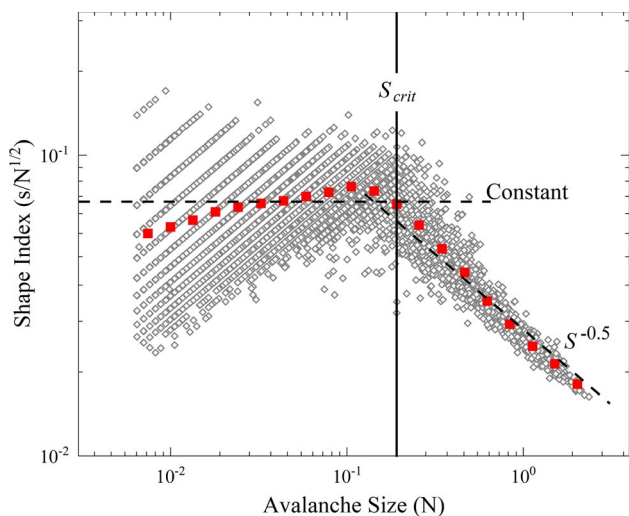


Fig. 3 Shape index α for granular materials. The shape index is roughly constant for the small avalanches. The minor drift of the shape index from the constant value in the small avalanche regime is most likely caused by the discrete durations of the small avalanches very close to the experimental detection threshold. Above the critical size ($S > 0.2$ N), we see an approximate $-1/2$ power-law dependence. The squares indicate the average shape index in one of 20 size bins. 95% error bars are on the order of the marker size

the large avalanches in both BMGs and granular material. Small avalanches are self-similar with the same dynamics for many sizes, as indicated by the constant α , but large avalanches are not. For large avalanches, events of different sizes will have different dynamics, and this will be indicated by a difference in α . Temporal avalanche profiles of large avalanches, averaged over narrow size ranges, are shown in Figs. 4a and 5a for BMGs and the granular material, respectively. Figures 4b and 5b show the average stress-drop rate normalized by the maximum average stress drop rate and time divided by the square root of the avalanche size S for the same average shapes as in Figs. 4a and 5a. Rescaling the shapes in this way shows the change in the functional form of the avalanche peak width from broad to narrow as α decreases in both systems.

The size index for the shapes is also indicated in Figs. 4 and 5. These large avalanches span a range of shape indices in both materials. In avalanches with the smallest sizes of those shown, which correspond to the largest values of α , we see the avalanche profiles, the “shapes,” have wide peaks. The stress drop rate is on the order of the maximum stress drop rate for the large majority of the duration. This indicates that a large proportion of cells are failing, relative to the proportion of cells that fail at the fastest part of the event,

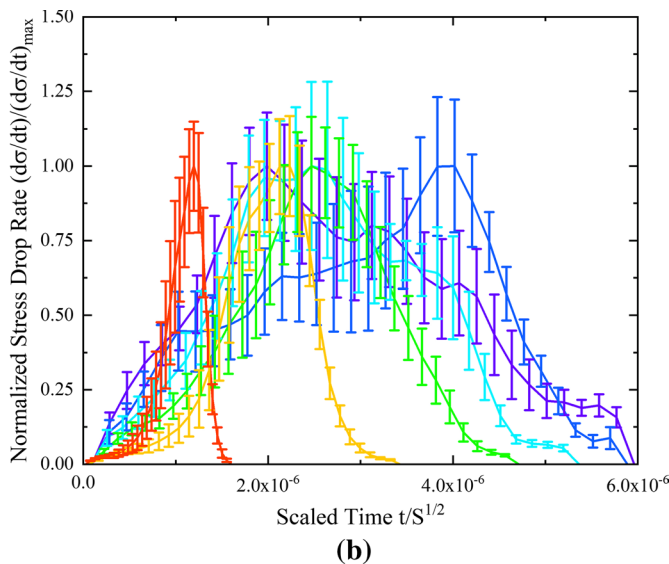
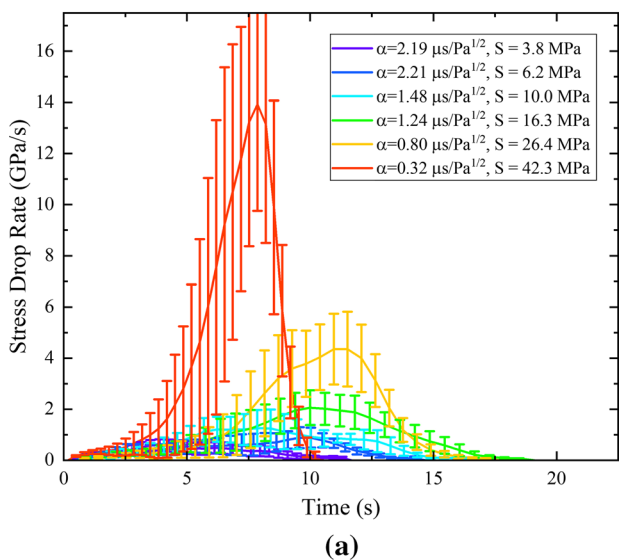


Fig. 4 a Average stress drop rate $\langle -d\sigma/dt \rangle_S(t)$ averaged over avalanches of similar size as a function of time (i.e., the “shape” for a given avalanche size) for large avalanches in BMGs (from large to small α , the number of events averaged to produce each shape is 7, 5, 8, 14, 8, and 7). A smaller shape index α , coincident with a larger size S , indicates a sharp peak that lasts only a portion of the total duration. The peak represents a period of fast propagation during which many cells fail. The avalanches with small shape indices show more pronounced peaks than those with large shape indices. Avalanches are considered “large” above a critical size S_{crit} of ~ 2 MPa.

b Rescaled stress-drop rate profiles (scaling functions) $G(x)$ of Eqs. (1) and (2) for the same events as in a. Each average stress-drop rate profile in a is divided by the maximum average stress drop rate $M \equiv \langle -d\sigma/dt \rangle_{max}$ and time is divided by the square root of the avalanche size S . The large events have a smaller peak width. Despite the noise, the smaller avalanches have wider shapes $G(x)$ than the larger ones. The large error bars are due to the presence of only a few events in each bin. Error bars indicate 95% confidence intervals in both a and b. Color is consistent between both a and b (color figure online)

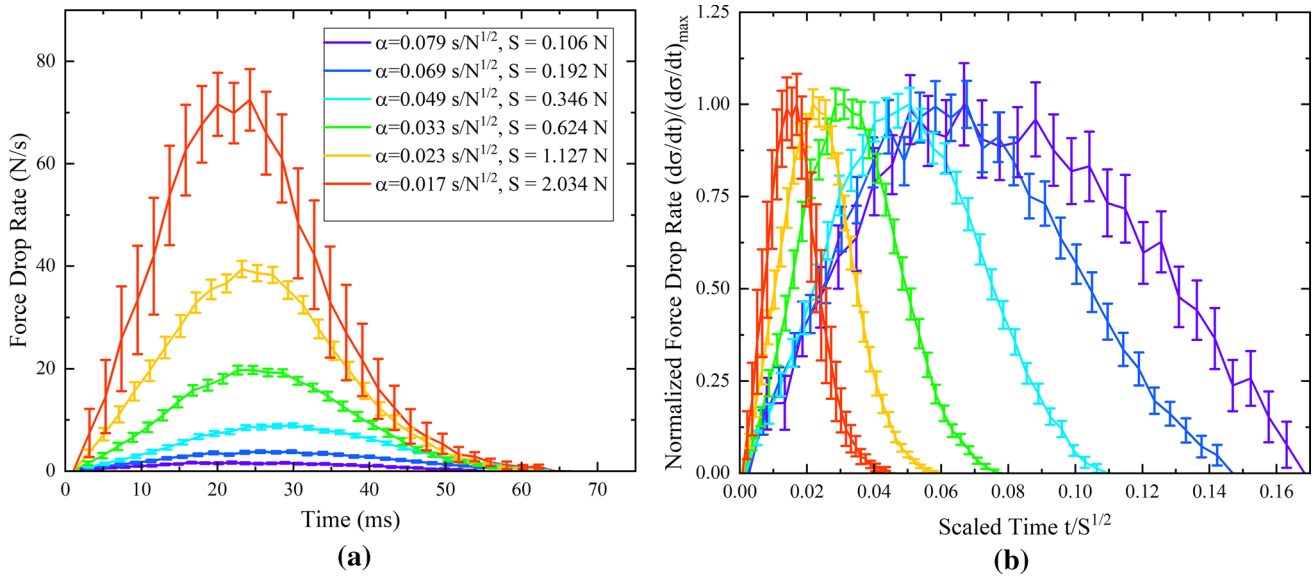


Fig. 5 a Average force drop rate as a function of time (i.e., the “shape”) for large avalanches in granular materials (from large to small α , the number of events averaged to produce each shape is 221, 234, 179, 195, 179, and 18). A smaller shape index α , coincident with a larger size S , indicates a sharp peak that lasts only a portion of the total duration. The peak represents a period of fast propagation during which many cells fail. Just like for BMGs, the avalanches with small shape indices show more pronounced peaks than those with large shape indices. Avalanches are considered “large” above a criti-

cal size S_{crit} of $\sim 0.2 \text{ N}$. The shown shapes are the temporal profiles of the force drop rates averaged over many avalanches of similar size. **b** Rescaled stress-drop rate profiles $G(x)$ of Eqs. (1) and (2) for the same events as in **a**. Each average stress-drop rate profile in **a** is divided by the maximum average stress drop rate $M \equiv \langle -d\sigma/dt \rangle_{\max}$ and time is divided by the square root of the avalanche size S . Error bars indicate 95% confidence intervals in both **a** and **b**. Color is consistent between both **a** and **b**

throughout the avalanche. In contrast, the largest events shown, i.e., those with the smallest values of α , show sharp peaks in their shapes. Those shapes have extended periods where the stress drop rate is much lower than the maximum at the beginning and end of the avalanche. In these periods, there are few cells failing, again relative to the number at the fastest part. The majority of the stress drop happens very quickly and only in a portion of the total avalanche; these periods are the peaks. We can see that there is a clear difference between the dynamics of events of different sizes, and furthermore, that these differences are shared by BMGs and granular media. As expected, α does change as the dynamics change in both systems. α characterizes how peaked the shapes are and can therefore serve to differentiate types of propagation.

Finally, the model also predicts spatial scaling of the avalanches. The mean-field model predicts that small avalanches propagate in a pulse-like fashion with approximately the same displacement at every slipping region. Consequently, the total slip S scales linearly with the slipping area A , i.e., $S \sim A$, causing the small avalanches to increase in both size and duration. The large avalanches, however, are system-spanning. They propagate simultaneously across the entire specimen. Thus the mean-field model predicts that the total integrated displacement in a large avalanche grows with the slipping area to the $3/2$

power, i.e., $S \sim A^{3/2}$, which is the same dependence as seen in cracks. In summary,

$$S \sim \begin{cases} A, & S < S_{crit} \\ A^{3/2}, & S > S_{crit} \end{cases} \quad (5)$$

This scaling behavior reflects the difference in the propagation mechanism between small and large avalanches. An experiment that measures the amount of slip A associated with each avalanche of known size S should reveal these different scaling behaviors of small and large avalanches. While the current data have no spatial resolution, we can use the mean-field model to predict the scaling in space of the avalanches.

3 Conclusion

Both BMGs and granular systems show similar differences between small and large avalanches, specifically in their relationship between the avalanche sizes and durations, and the avalanche sizes and maximum stress drop rates. We have developed a metric for avalanches that both encapsulates these relationships and describes the dynamics of the avalanches. The dynamics clearly differ for the

small avalanches that have power-law statistics compared to the dynamics of the large avalanches that do not.

The differences between small and large avalanches are consistent with the predictions of a simple model for slip avalanches in solids and granular materials [6, 15]. This model predicts that the small avalanches propagate in a pulse-like fashion with intermittent acceleration and deceleration throughout the pulse. In contrast, the large avalanches are predicted to propagate in a crack-like fashion, with a smooth acceleration to high rates that small avalanches can never reach. For small avalanches, the total slip (and thus the total stress drop) is predicted to scale linearly with the slipping area. For the large avalanches, however, the slipping area is predicted to be connected and system-spanning, and the total slip scales to the $3/2$ power of the slipping area. It would be instructive and interesting to see a comparison of these predictions with spatio-temporally resolved experiments for a wide range of materials.

Acknowledgements We thank Bob Behringer for many extremely helpful discussions and his kind encouragement through the years. WJW gratefully acknowledges the Heinemann Family Professorship at Bucknell University. KAD thanks the Guggenheim Foundation, MGA, and NSF CBET 1336634 for support. TCH gratefully acknowledges support from NSF DMR 1408686. WJW and KAD also thank the Kavli Institute for Theoretical Physics for hospitality and support under NSF PHY17-48958. PS acknowledges support by a Vici fellowship from the Netherlands Organization for Scientific Research (NWO).

Compliance with ethical standards

Conflict of interest The authors declare that they have no conflicts of interest.

Open Access This article is distributed under the terms of the Creative Commons Attribution 4.0 International License (<http://creativecommons.org/licenses/by/4.0/>), which permits unrestricted use, distribution, and reproduction in any medium, provided you give appropriate credit to the original author(s) and the source, provide a link to the Creative Commons license, and indicate if changes were made.

References

- Antonaglia, J., Wright, W.J., Gu, X.J., Byer, R.R., Hufnagel, T.C., LeBlanc, M., Uhl, J.T., Dahmen, K.A.: Bulk metallic glasses deform via slip avalanches. *Phys. Rev. Lett.* **112**, 155501 (2014)
- Antonaglia, J., Xie, X., Schwarz, G., Wraith, M., Qiao, J., Zhang, Y., Liaw, P.K., Uhl, J.T., Dahmen, K.A.: Tuned critical avalanche scaling in bulk metallic glasses. *Sci. Rep.* **4**, 4382 (2014)
- Uhl, J.T., Pathak, S., Schorlemmer, D., Liu, X., Swindeman, R., Brinkman, B.A.W., LeBlanc, M., Tsekenis, G., Friedman, N., Behringer, R., Denisov, D., Schall, P., Gu, X.J., Wright, W.J., Hufnagel, T., Jennings, A., Greer, J.R., Liaw, P.K., Becker, T., Dresen, G., Dahmen, K.A.: Universal quake statistics: from compressed nanocrystals to earthquakes. *Sci. Rep.* **5**, 16493 (2015)
- Denisov, D.V., Lörincz, K.A., Uhl, J.T., Dahmen, K.A., Schall, P.: Universality of slip avalanches in flowing granular matter. *Nat. Commun.* **7**, 10641 (2016)
- Denisov, D.V., Lörincz, K.A., Wright, W.J., Hufnagel, T.C., Nawano, A., Gu, X.J., Uhl, J.T., Dahmen, K.A., Schall, P.: Universal slip dynamics in metallic glasses and granular matter—linking frictional weakening with inertial effects. *Sci. Rep.* **7**, 43376 (2017)
- Dahmen, K.A., Ben-Zion, Y., Uhl, J.T.: A simple analytic theory for the statistics of avalanches in sheared granular materials. *Nat. Phys.* **7**, 554 (2011)
- Zhang, Y., Zuo, T.T., Tang, Z., Gao, M.C., Dahmen, K.A., Liaw, P.K., Lu, Z.P.: Microstructures and properties of high-entropy alloys. *Progr. Mater. Sci.* **61**, 1 (2014)
- Friedman, N., Jennings, A.T., Tsekenis, G., Kim, J.-Y., Tao, M., Uhl, J.T., Greer, J.R., Dahmen, K.A.: Statistics of dislocation slip avalanches in nanosized single crystals show tuned critical behavior predicted by a simple mean field model. *Phys. Rev. Lett.* **109**, 095507 (2012)
- Sparks, G., Maaß, R.: Shapes and velocity relaxation of dislocation avalanches in Au and Nb microcrystals. *Acta Mater.* **152**, 86 (2018)
- Fisher, D.S., Dahmen, K.A., Ramanathan, S., Ben-Zion, Y.: Statistics of earthquakes in simple models of heterogeneous faults. *Phys. Rev. Lett.* **78**, 4885 (1997)
- Miguel, M.-C., Vespignani, A., Zapperi, S., Weiss, J., Grasso, J.-R.: Intermittent dislocation flow in viscoplastic deformation. *Nature* **410**, 667 (2001)
- Koslowski, M., LeSar, R., Thomson, R.: Avalanches and scaling in plastic deformation. *Phys. Rev. Lett.* **93**, 125502 (2004)
- Dimiduk, D.M., Woodward, C., LeSar, R., Uchic, M.D.: Scale-free intermittent flow in crystal plasticity. *Science* **312**, 1188 (2006)
- Zaiser, M.: Scale invariance in plastic flow of crystalline solids. *Adv. Phys.* **55**, 185 (2006)
- Dahmen, K.A., Ben-Zion, Y., Uhl, J.T.: Micromechanical model for deformation in solids with universal predictions for stress-strain curves and slip avalanches. *Phys. Rev. Lett.* **102**, 175501 (2009)
- Maaß, R., Derlet, P.M., Greer, J.R.: Small-scale plasticity—insights into dislocation avalanche velocities. *Scr. Mater.* **69**, 568 (2013)
- Ispánovity, P.D., Laurson, L., Zaiser, M., Groma, I., Zapperi, S., Alava, M.J.: Avalanches in 2D dislocation systems: plastic yielding is not depinning. *Phys. Rev. Lett.* **112**, 235501 (2014)
- Wright, W.J., Liu, Y., Gu, X.J., Van Ness, K.D., Robare, S.L., Liu, X., Antonaglia, J., LeBlanc, M., Uhl, J.T., Hufnagel, T.C., Dahmen, K.A.: Experimental evidence for both progressive and simultaneous shear during quasistatic compression of a bulk metallic glass. *J. Appl. Phys.* **119**, 084908 (2016)
- Papanikolaou, S., Cui, Y., Ghoniem, N.: Avalanches and plastic flow in crystal plasticity: an overview. *Model. Simul. Mater. Sci. Eng.* **26**, 013001 (2017)
- Pan, Y., Wu, H., Wang, X., Sun, Q., Xiao, L., Ding, X., Sun, J., Salje, E.K.H.: Rotatable precipitates change the scale-free to scale dependent statistics in compressed Ti nano-pillars. *Sci. Rep.* **9**, 3778 (2019)
- Pelusi, F., Sbragaglia, M., Benzi, R.: Avalanche statistics during coarsening dynamics. *Soft Matter* **15**, 4518 (2019)
- Romero, F.J., Martín-Olalla, J.-M., Gallardo, M.C., Soto-Parra, D., Salje, E.K.H., Vives, E., Planes, A.: Scale-invariant avalanche dynamics in the temperature-driven martensitic transition of a Cu–Al–Be single crystal. *Phys. Rev. B* **99**, 224101 (2019)
- Song, H., Dimiduk, D., Papanikolaou, S.: Universality class of nanocrystal plasticity: localization and self-organization in discrete dislocation dynamics. *Phys. Rev. Lett.* **122**, 178001 (2019)

24. Zreihan, N., Faran, E., Vives, E., Planes, A., Shilo, D.: Relations between stress drops and acoustic emission measured during mechanical loading. *Phys. Rev. Mater.* **3**, 043603 (2019)
25. Cao, P., Dahmen, K.A., Kushima, A., Wright, W.J., Park, H.S., Short, M.P., Yip, S.: Nanomechanics of slip avalanches in amorphous plasticity. *J. Mech. Phys. Solids.* **114**, 158 (2018)
26. LeBlanc, M., Nawano, A., Wright, W.J., Gu, X.J., Uhl, J.T., Dahmen, K.A.: Avalanche statistics from data with low time resolution. *Phys. Rev. E* **94**, 051235 (2016)
27. Barés, J., Wang, D., Wang, D., Bertrand, T., O'Hern, C.S., Behringer, R.P.: Local and global avalanches in a two-dimensional sheared granular medium. *Phys. Rev. E* **96**, 052902 (2017)
28. Murphy, K.A., Dahmen, K.A., Jaeger, H.M.: Transforming mesoscale granular plasticity through particle shape. *Phys. Rev. X* **9**, 011014 (2019)
29. Nicolas, A., Ferrero, E.E., Martens, K., Barrat, J.-L.: Deformation and flow of amorphous solids: insights from elastoplastic models. *Rev. Mod. Phys.* **90**, 045006/1-63 (2018)

Publisher's Note Springer Nature remains neutral with regard to jurisdictional claims in published maps and institutional affiliations.